Journal of Power Sources 252 (2014) 138–143

Contents lists available at ScienceDirect

Journal of Power Sources

journal homepage: www.elsevier.com/locate/jpowsour

Improved high-temperature performance of lithium-ion batteries through use of a thermally stable co-polyimide-based cathode binder

Jaecheol Choi [a,2], Myung-Hyun Ryou [a,2], Bongki Son [a], Jongchan Song [b], Jung-Ki Park [b], Kuk Young Cho [c,1], Yong Min Lee [a,*]

[a] Department of Chemical and Biological Engineering, Hanbat National University, Deokmyoung-dong, Yuseong-gu, Daejeon 305-719, Republic of Korea
[b] Department of Chemical and Biomolecular Engineering, Korea Advanced Institute of Science and Technology, Guseong-dong, Yuseong-gu, Daejeon 305-701, Republic of Korea
[c] Division of Advanced Materials Engineering, Kongju National University, 275 Budae-dong, Cheonan, Chungnam 331-717, Republic of Korea

HIGHLIGHTS

- Co-polyimide binders improve high temperature cell performances of LIBs.
- Adhesion strength within cathode electrodes is related to cell performance of LIBs.
- Co-polyimide binders enhance adhesion strength within cathode electrodes.

ARTICLE INFO

Article history:
Received 8 October 2013
Received in revised form
3 December 2013
Accepted 4 December 2013
Available online 12 December 2013

Keywords:
Co-polyimide
High-temperature stability
Cathode binder
High temperature
Lithium-ion batteries

ABSTRACT

The effects of a thermally stable co-polyimide-based polymeric binder on the performance of a cathode electrode are investigated. The introduction of co-polyimide (P84) into a conventional polymeric binder system based on polyvinylidene fluoride (PVdF) enhances the cycle performance under high-temperature conditions (60 °C). Because of the inherent mechanical and thermal stabilities of the co-polyimide, P84 retains outstanding adhesive/cohesive strength within the electrode composite, as well as between the electrode composite and the aluminum current collector. These findings are further supported by electrochemical impedance spectroscopic analysis, scanning electron microscope, and studies using a Surface and Interfacial Cutting Analysis System (SAICAS®).

1. Introduction

Lithium-ion batteries (LIBs) are the predominantly used power sources in portable electronic devices. They are now being extensively investigated as potential power sources for large-scale applications such as electric vehicles (EVs) because of their high energy densities and good round-trip energy efficiency [1–3]. However, large-scale LIBs remain economically uncompetitive on account of their poor performance at low and high temperatures (around 50 °C), safety issues, and high costs [4–7]. In contrast to portable electronic devices, EVs must endure abusive operating and survival conditions because the vehicles are exposed to outdoor settings for significant periods of time. As local climates vary profoundly, there are significant temperature differences between regions and countries. Consequently, to guarantee reliable LIB performance to customers, the FreedomCAR Battery Test Manual stipulates that large-scale LIBs for EVs must survive over a wide range of temperatures, between −46 and 66 °C [7].

High temperatures (around 50 °C) can significantly degrade the performance and reliability of LIBs and can even cause thermal runaway, which is a serious, threatening safety issue [6,8,9]. High-temperature storage causes various chemical and electrochemical reactions associated with the cathode, anode, and electrolyte, which in turn result in surface layer changes that hinder the

* Corresponding author. Tel.: +82 42 821 1549; fax: +82 42 821 1692.
E-mail addresses: kycho@kongju.ac.kr (K.Y. Cho), yongmin.lee@hanbat.ac.kr (Y. M. Lee).
[1] Tel.: +82 41 521 9398; fax: +82 568 5776.
[2] These authors contributed equally to this work.

0378-7753/$ – see front matter © 2013 Published by Elsevier B.V.
http://dx.doi.org/10.1016/j.jpowsour.2013.12.015

diffusion of Li ions and reduce the utilization of the active material [10–12]. Consequently, LIBs exposed to high-temperature conditions (around 50 °C) show severe power and/or capacity fades during prolonged cycling. More importantly, LIBs operating under abusive conditions such as high current density charging and/or discharging processes may cause heat to be accumulated inside the batteries [13–15]. If LIBs generate more heat than that dissipated to the surroundings, battery temperatures can rise significantly and result in thermal runaway.

To alleviate the performance decay of LIBs under high-temperature conditions, various studies have focused on the mechanisms of LIB failure during storage and operation under high-temperature conditions associated with the cathode [16–18], anode [4,19–21], and electrolyte [22–24]. Among these, the polymeric binder materials used in commercialized cathode electrodes seem to be one of the dominant failure mechanisms of LIBs under high-temperature conditions, as recently suggested by Oh's group [25]. Polyvinylidene fluoride (PVdF) is widely used as a polymeric binder material for cathode materials. Recently, it was reported that PVdF is easily loosened or weakened under high-temperature conditions, losing the mechanical strength to tie together the electrode constituents such as the active materials, electric conducting agent, and current collector [25]. This results in a breakdown of the electrical conductive network between the electrode constituents, and consequently leads to irretrievable performance degradation of the LIBs. Furthermore, PVdF expedites thermal runaway at high temperatures owing to its low melting point and a combination of thermal decomposition reactions associated with lithium ions [26].

In order to mitigate this pivotal problem regarding the commercialized PVdF polymeric binder material of the cathode electrode, we suggest its replacement with the thermally stable co-polymerized polyimide P84 (3,3,4,4-benzophenone-tetracarboxylic dianhydride (BTDA), with 80% toluene diisocyanate (TDI) and 20% methylene diphenyl diisocyanate (MDI)), which is soluble in common solvents and is heat resistant. As an extension of our previous work in which P84 was used as a separator coating material [27], P84 seemed to be appropriate for the binder material of cathode electrodes because it is electrochemically stable up to 4.8 V versus Li/Li^+. We monitored the cycle performance of the LIBs at a high temperature (60 °C), and correlated the relationship between the mechanical properties of the polymeric binder and its cycle performance by evaluating the shear stress and adhesion/cohesion force with respect to the electrode composite using a surface and interfacial cutting analysis system (SAICAS®).

2. Experimental

2.1. Cathode preparation

Cathodes were prepared by coating *N*-methyl-*2*-pyrrolidone-based slurry (NMP, Sigma–Aldrich, USA) consisting of 90 wt% $LiCoO_2$ (10 μm, KD-10, Umicore, Korea), 5 wt% conductive carbon (Super-P, Timcal, Switzerland), and 5 wt% polyvinylidene fluoride (PVdF, KF-1300, Kureha Battery Materials Co., Japan, $M_w = 350{,}000$) polymeric binder onto Al current collector foil (15 μm, Sam-A Aluminium Co., LTD., Korea). The dual polymeric binder solution was prepared by dissolving PVdF and co-polyimide (P84, HP Polymer GmbH, Austria, M_w = 150,000) in NMP (10/0 and 9/1 w/w, respectively) [27]. The cast slurry was dried in oven at 130 °C for 30 min, and then roll-pressed with a gap-control-type roll-pressing machine (CLP-2025, CIS, Korea). The cathode loading was about 8 mg cm^{-2}, and the thickness and density were controlled to be 35 μm and 2.4 g cm^{-3}, respectively.

2.2. Cell assembly

The cathodes employing PVdF and/or P84 binder were cut into disk shapes (radius: 12 mm) and assembled into 2032-type coin half cells using Li-metal (450 μm, Honjo Metal Co., Japan, radius: 16.2 mm) as the counter and reference electrodes and polyethylene (PE) separators (thickness: 20 μm, radius: 18 mm, ND420, Asahi Kasei E-materials, Japan). A mixture containing 1.15 M lithium hexafluorophosphate ($LiPF_6$) in ethylene carbonate (EC)/ethyl methyl carbonate (EMC) (3/7 v/v, PANAX ETEC, Korea) was used as an electrolyte. All cell assembly and disassembly processes were conducted in an argon-filled glove box, in which the dew point was maintained at less than −80 °C.

2.3. Electrochemical testing

After aging for 12 h, the coin cells were cycled as a formation step between 3.0 and 4.2 V at a constant current (CC) in both charging and discharging processes at a C/10 rate and at 25 °C using a charge/discharge cycler (PNE Solutions, Korea). To stabilize the cells, they were cycled between 3.0 and 4.2 V at a slightly higher current density at a C/5 rate for an additional 3 cycles. These two steps were designated as precycling. Thereafter, the cells were cycled at 25 °C and 60 °C with a constant current density at the C/2 rate. The AC impedance of the cells after precycling and cycle tests was determined using a VSP impedance analyzer (Bio-Logic SAS, France) over the frequency range 1 MHz–50 mHz at an amplitude of 10 mV.

2.4. Post-mortem testing

The cross-sectional morphologies of the cathodes after cycling were characterized by field-emission scanning electron microscopy (FE-SEM, S4800, Hitachi, Japan). To prepare cross-sectional specimens, each cathode was cut by an argon-ion beam polisher (E3500, Hitachi) at a constant power of 2.1 W (6 kV and 0.35 mA) under vacuum ($<2.0 \times 10^{-4}$ Pa).

2.5. Shear stress and adhesion/cohesion measurement

The shear stress of the electrode and the adhesion/cohesion strength between the cathode electrode composite and the current collector were measured using a Surface and Interfacial Cutting Analysis System (SAICAS®, Daipla Wintes Co., Ltd., Japan). For the SAICAS® measurements, a boron nitride blade (width: 1 mm) fixed at a 45° shear angle was used. During the test, the blade moved in the horizontal direction at 0.05 μm s^{-1}. The blade was also driven in the vertical direction, maintaining a vertical force of 0.5 N, until it reached the aluminum current collector. Thereafter, however, the vertical force was changed to 0.2 N to prevent movement in the vertical direction.

3. Results and discussion

Fig. 1 shows the potential profiles during the first charging and discharging processes for the cells employing pure PVdF as the cathode binder (hereafter referred to as PVdF) and those employing a mixture of 90 wt% PVdF and 10 wt% P84 as the cathode binder (hereafter referred to as PVdF/P84). Both cells demonstrated similar electrochemical profiles, which nearly overlapped, indicating that both cathode polymeric binder materials work comparably well in the formation step (Coulombic efficiency: 97.1%, 136.3 mAh g^{-1} for PVdF, *vs.* 97.1%, 136.4 mAh g^{-1} for P84). The AC impedance spectra also supported these results, demonstrating nearly identical results for both cases, as seen in Fig. 2. Judging from the preliminary test as

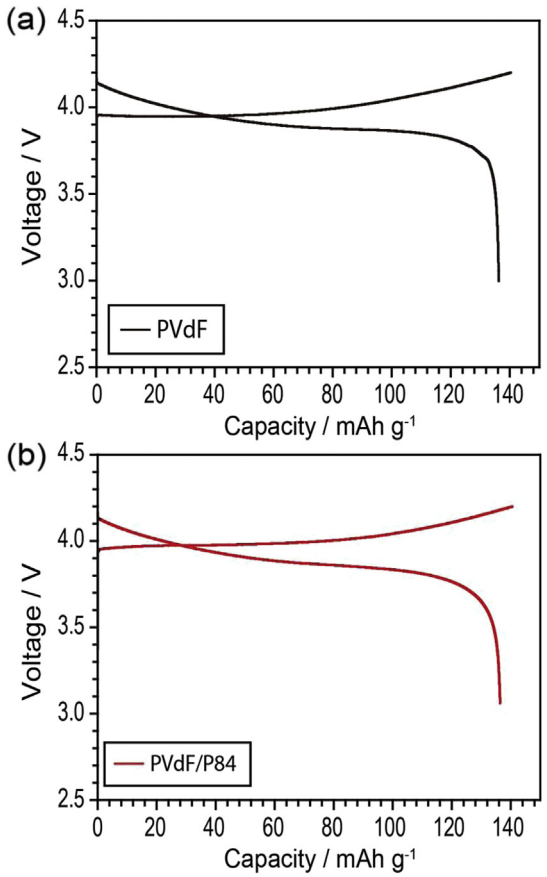

Fig. 1. Voltage profiles of the cells employing (a) PVdF and (b) PVdF/P84 polymeric binders during the first cycle (C/10 rate, 0.11 mA cm^{-2}, during charging and discharging processes between 3.0 and 4.2 V *vs.* Li/Li^+ at 25 °C).

varying the P84 ratio from 0 to 20 wt%, a polymer blend consisting of 10 wt% P84 and 90 wt% PVdF seemed to be a promising choice for the cathode polymeric binder, which increases the thermal stability of the LIBs at high temperature operating condition (60 °C) without impeding rate capability and increasing battery cost.

The cycle performances of the cells were evaluated both at room temperature (25 °C) and high temperature (60 °C). Although both cells revealed nearly similar cycle performances at room temperature (Fig. 3(a), 95.0%, 130.8 mAh g^{-1} for PVdF, 96.1%, 131.6 mAh g^{-1} for PVdF/P84 after 200 cycles), the cells employing PVdF/P84 remarkably enhanced the discharge capacity retention abilities by ~120% at high temperatures after 200 cycles, as compared to those employing PVdF (Fig. 3(b), 78.9%, 110.4 mAh g^{-1} for PVdF, 94.8%, 132.8 mAh g^{-1} for PVdF/P84 after 200 cycles). Clearly, as seen in the voltage profiles for the cells of different cycles (Fig. 4), serious discharge capacity fading was observed in the cells employing PVdF, while no obvious change was noted in the PVdF/P84 case.

To further analyze the role of P84 as a cathode binder, we monitored the interfacial resistance changes, i.e., the AC impedance, via electrochemical impedance spectroscopy (EIS) measurements. Polarization in the cell is closely related to the capacity decay of the cells, and thus could be an important index for evaluating the electrode properties [25,28,29]. We speculate that the arcs below 10 Hz for 50 and 100 cycles in Fig. 5(a) corresponds to the diffusion parameters of the electrodes [30], while the other depressed semi-circles both in Fig. 5(a) and (b) below 10 Hz seem to be attributed to charge-transfer through the electrode/electrolyte interface [31]. Keeping these in mind, as observed in Fig. 5, the cells employing PVdF exhibited drastic impedance increases concurrently with cycling, while those employing PVdF/P84 showed moderate impedance increases. Considering the impedance results associated with the cycle performance of the cells shown in Figs. 3 and 4, we could speculate that P84 successfully controlled the polarization increase inside of the cell, which

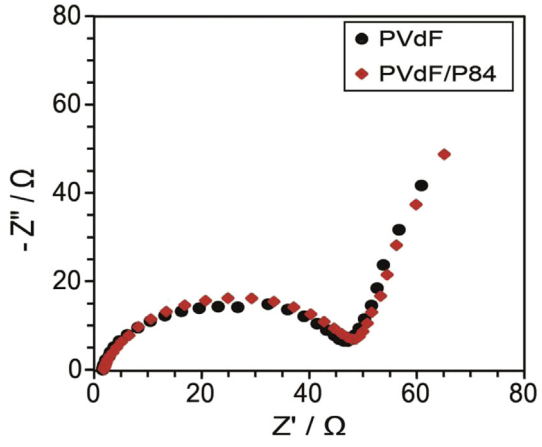

Fig. 2. Nyquist plots for the cells employing PVdF and PVdF/P84 polymeric binders after the first cycle.

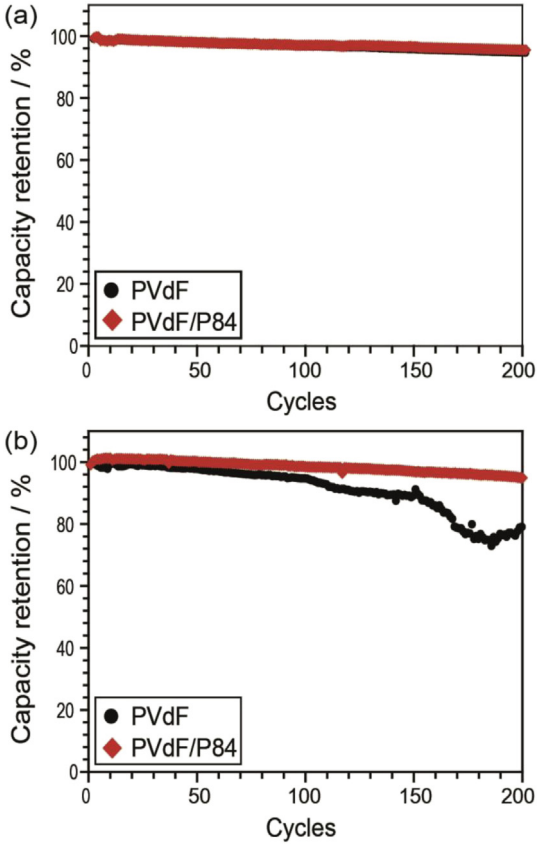

Fig. 3. Cycle performances of the cells employing PVdF and PVdF/P84 polymeric binders operated at (a) 25 °C and (b) 60 °C (C/2 rate, 0.55 mA cm^{-2}, during charging and discharging processes between 3.0 and 4.2 V *vs.* Li/Li^+).

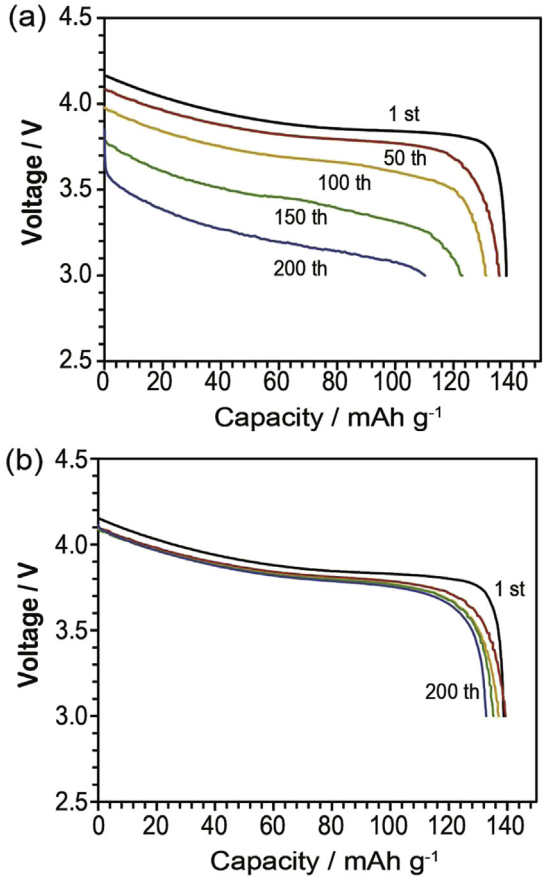

Fig. 4. Comparison of voltage profiles of cells in Fig. 3(b) employing (a) PVdF and (b) PVdF/P84 at different cycles (C/2 rate, 0.55 mA cm^{-2}, during charging and discharging processes between 3.0 and 4.2 V *vs.* Li/Li^+ at 60 °C).

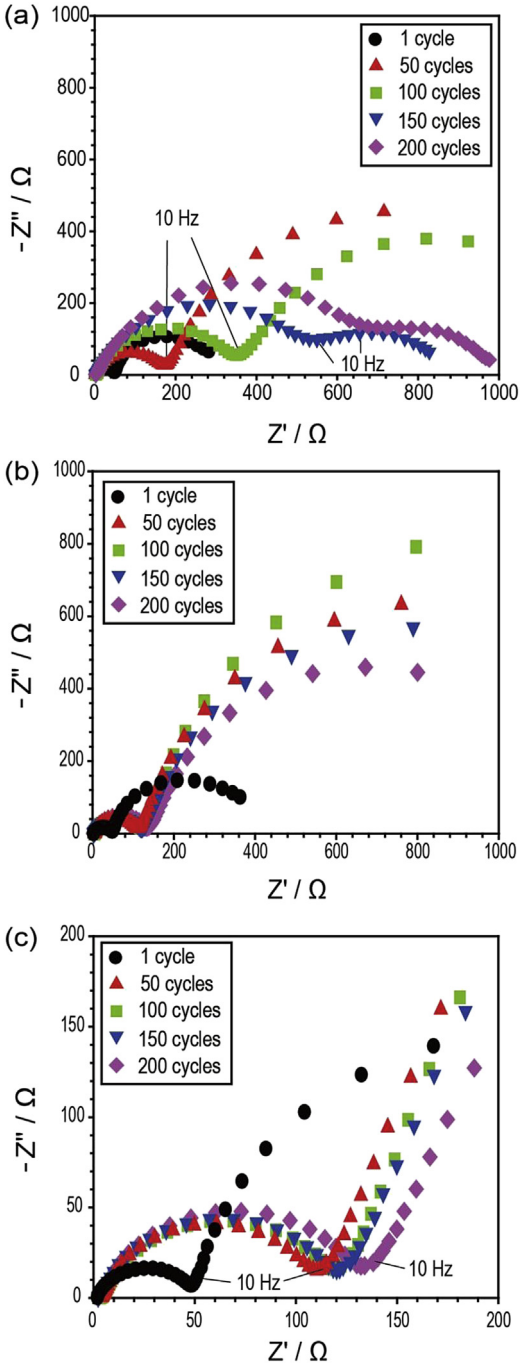

Fig. 5. Nyquist plots of cells in Fig. 3(b) employing (a) PVdF, (b) PVdF/P84 and (c) enlarged figure of Fig. 5(b) at different cycles (C/2 rate, 0.55 mA cm^{-2}, during charging and discharging processes between 3.0 and 4.2 V *vs.* Li/Li^+ at 60 °C).

mitigated cycle performance decay under high temperature conditions (60 °C).

To evaluate the relationship between the cycle performance and the mechanical properties of the cathode electrodes, we monitored the morphological changes of the cathode electrode and evaluated the shear stress and adhesion/cohesion forces associated with the polymeric binders via post-mortem experiments. For sample preparation, fully discharged cells (~3.0 V *vs.* Li/Li^+) were disassembled in a glove box under argon after the cycling tests.

Scanning electron microscope (SEM) cross-sectional images of the cathode electrodes (Fig. 6 (a) and (b)) revealed very similar morphological structures of the PVdF and PVdF/P84 cathode electrodes before electrochemical experiments. After the high-temperature experiment, the PVdF cell exhibited a poor adhesion force between the electrode composite and the aluminum current collector, resulting in the detachment of the electrode composite from the current collector during the disassembly process; this was reproducible in repeated trials (Fig. 6(c)). In contrast, however, the PVdF/P84 was still well attached on the aluminum current collector after the disassembly process (Fig. 6(d)), which implies that the P84 adhesion force was much larger as compared to that in the case of PVdF. Because of its low glass transition temperature (about −34 °C *vs.* ~320 °C for P84), PVdF swells more easily in the electrolyte solution than does P84 and hence shows poor mechanical strength [32–34]. These observations are well consistent with the previous report describing poor cell performance under high-temperature conditions, ascribed to the breakdown of the electrically conductive network established between the active material, carbon, and the current collector when PVdF was used as the polymeric binder [25].

For a quantitative evaluation, we measured the adhesion force between the electrode composite and the current collector using SAICAS®. Generally, the peel test method is used for evaluating the adhesion properties of polymeric binder materials on electrodes [35–37]. In this method, the electrode sample is attached to 3 M tape, and the peel strength of the specimen is measured as the tape is pulled at 180° between the tape and the current collector at a constant displacement rate. Technically, however, this method can only evaluate the adhesion/cohesion strength of the polymeric

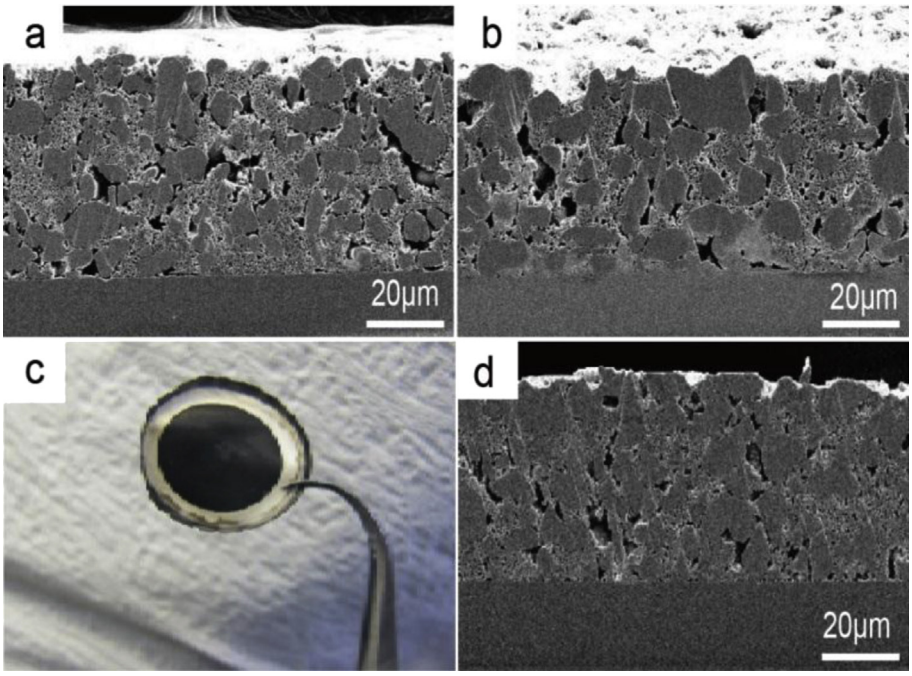

Fig. 6. Cross-sectional SEM images of pristine cathode electrodes employing (a) PVdF and (b) PVdF/P84 polymeric binders. (c) A digital camera image of separator with PVdF electrode composite, which were detached from the aluminum current collector during a cell disassembly process. (d) A cross-sectional SEM image of PVdF/P84 based electrode after cell operation (after 200 cycles at 60 °C in Fig. 3(b)).

binder within the electrode composite, implying that this is an unsuitable method to clearly measure the adhesion/cohesion strength between an electrode composite and the current collector. In contrast to the peel test method, by monitoring the vertical and horizontal interacting forces at a blade during sample cutting, SAICAS® can measure two interaction criteria: 1) the shear stress of the electrode composite, which reflects the adhesion/cohesion strength within the electrode composite, and 2) the adhesion/cohesion strength between the electrode composite and the current collector. The shear stress of the electrode composite can be preferentially evaluated by measuring the horizontal force reaction during the cutting of the electrode composite (cutting mode) [38]. After the blade reaches the interface between the electrode composite and the current collector, it moves forward only in the horizontal direction (peel mode), and thus, can evaluate the adhesion/cohesion strength between the electrode composite and current collector.

From the ratio of the measured horizontal force (F_H), the width of the blade (w), the electrode composite thickness (d), and the shear angle (φ), the shear stress and adhesion/cohesion strength can be obtained as follows [38,39];

$$\tau = F_H/(2w \cdot d \cdot \cot\varphi) \quad (\mathrm{MPa}) \tag{1}$$

$$P = F_H/w \quad \left(\mathrm{kN\ m^{-1}}\right) \tag{2}$$

Fig. 7 represents the total profiles of the interacting forces of the SAICAS® experiments for cathode electrodes employing PVdF and P84. We denoted section *A* and section *B* in the profiles, representing the "cutting mode" and "peel mode," in order to calculate the shear stress within the electrode composite and the adhesion/cohesion strength between the electrode composite and the current collector, respectively.

Using Equation (1) and the F_H obtained in section *A*, we obtained the shear stress (τ) of the cathode electrode composite. As summarized in Fig. 8(a), τ for the electrode composite using PVdF/P84 was ~200% higher than that of PVdF at the maximum value (0.0895 MPa *vs*. 0.0449 MPa, respectively) and ~200% higher at the average value (0.067 MPa *vs*. 0.034 MPa, respectively) than that of PVdF. Then, based on Equation (2), we calculated the adhesive/cohesive strength (P) between the electrode composite and the

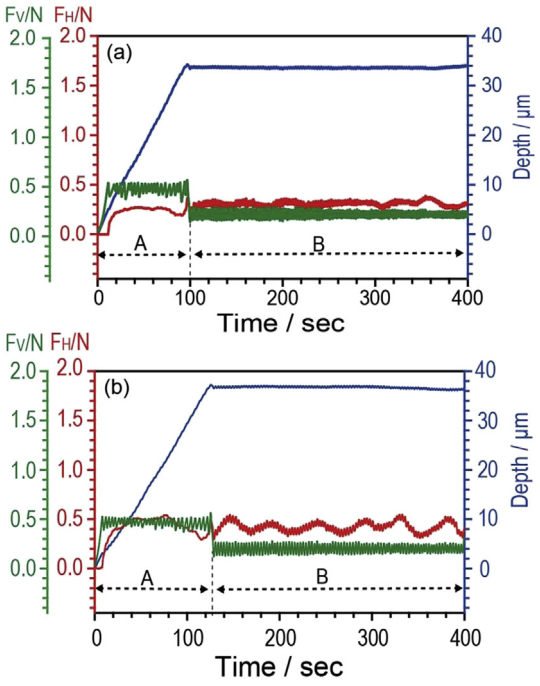

Fig. 7. Peeling test profiles of SAICAS® tests for cathode electrodes employing (a) PVdF and (b) PVdF/P84 polymeric binders (F_H: horizontal force, F_V: vertical force, D: depth distance).

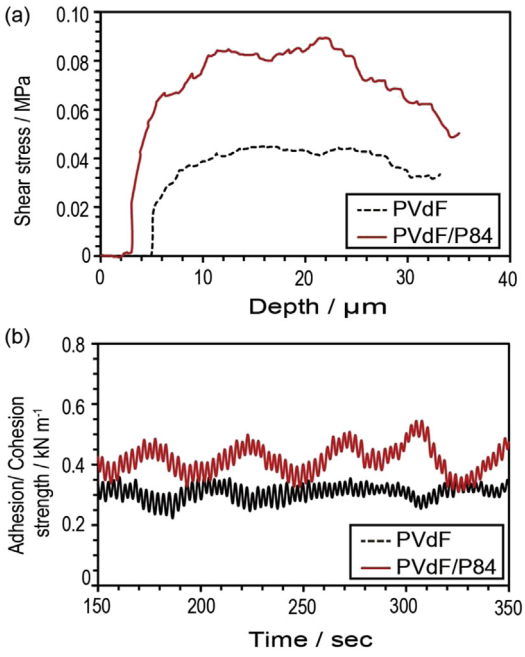

Fig. 8. Comparison of SAICAS® results of cathode electrodes employing PVdF and PVdF/P84 as a function of horizontal forces (F_H) during (a) cutting mode and (b) peel mode.

current collector using F_H value obtained in section *B* (peel mode). As seen in Fig. 8(b), *P* for P84 was ~150% higher at the maximum value (0.545 kN m^{-1} *vs.* 0.359 kN m^{-1}, respectively) and ~140% higher at the average value (0.416 kN m^{-1} *vs.* 0.307 kN m^{-1}, respectively) than that of PVdF. Considering these results, it is clear that P84 improved both τ and *P*. These findings may be attributed to the combination between higher glass transition temperature (T_g) of P84 compared to PVdF, which results in better mechanical interlocking within electrodes, and the chemical affinity with other electrode substituent to bind [33,34,40,41].

4. Conclusion

Introduction of the co-polyimide P84 into the binder material significantly improved the cycle performance of LIBs under high temperature conditions, especially at 60 °C, compared to the conventional pure polymeric binder (PVdF) system (94.8% *vs.* 78.9% of initial discharge capacity after 200 cycles for PVdF/P84 and PVdF, respectively). This enhancement in the cells employing P84 was ascribed to the better adhesion/cohesion properties of P84 within the electrode composite as well as between the electrode composite and the current collector. Using a SAICAS® experiment, the 10 wt% replacement of P84 into the PVdF-based cathode binder system revealed improvements in the shear stress and adhesion/cohesive strength of up to ~200% and ~150% of those of the PVdF system, respectively.

Acknowledgements

This research was financially supported by the National Research Foundation of Korea (NRF) through the Human Resource Training Project for Regional Innovation and Chungcheong Leading Industry Promotion Project of the Korean Ministry of Trade, Industry and Energy. The authors also thank Sungmoon Systech Corp. in Korea for SAICAS® measurement.

References

[1] L.-F. Cui, Y. Yang, C.-M. Hsu, Y. Cui, Nano Lett. 9 (2009) 3370–3374.
[2] B.M. Bang, J.I. Lee, H. Kim, J. Cho, S. Park, Adv. Energy Mater. 2 (2012) 878–883.
[3] B. Scrosati, J. Hassoun, Y.-K. Sun, Energy Environ. Sci. 4 (2011) 3287–3295.
[4] H. Yang, H. Bang, K. Amine, J. Prakash, J. Electrochem. Soc. 152 (2005) A73–A79.
[5] X. Yao, S. Xie, C. Chen, Q. Wang, J. Sun, Y. Li, S. Lu, J. Power Sources 144 (2005) 170–175.
[6] Q. Wang, P. Ping, X. Zhao, G. Chu, J. Sun, C. Chen, J. Power Sources 208 (2012) 210–224.
[7] E. Karden, S. Ploumen, B. Fricke, T. Miller, K. Snyder, J. Power Sources 168 (2007) 2–11.
[8] R. Sabbah, R. Kizilel, J. Selman, S. Al-Hallaj, J. Power Sources 182 (2008) 630–638.
[9] M.-H. Ryou, J.-N. Lee, D.J. Lee, W.-K. Kim, Y.K. Jeong, J.W. Choi, J.-K. Park, Y.M. Lee, Electrochim. Acta 83 (2012) 259–263.
[10] M.-S. Wu, P.-C.J. Chiang, J.-C. Lin, J. Electrochem. Soc. 152 (2005) A1041–A1046.
[11] J. Vetter, P. Novak, M. Wagner, C. Veit, K.-C. Möller, J. Besenhard, M. Winter, M. Wohlfahrt-Mehrens, C. Vogler, A. Hammouche, J. Power Sources 147 (2005) 269–281.
[12] M. Broussely, P. Biensan, F. Bonhomme, P. Blanchard, S. Herreyre, K. Nechev, R. Staniewicz, J. Power Sources 146 (2005) 90–96.
[13] S. Al Hallaj, H. Maleki, J. Hong, J. Selman, J. Power Sources 83 (1999) 1–8.
[14] K. Smith, C.-Y. Wang, J. Power Sources 160 (2006) 662–673.
[15] E. Meissner, G. Richter, J. Power Sources 144 (2005) 438–460.
[16] I. Belharouak, G.M. Koenig, T. Tan, H. Yumoto, N. Ota, K. Amine, J. Electrochem. Soc. 159 (2012) A1165–A1170.
[17] F. Jiao, J. Bao, A.H. Hill, P.G. Bruce, Angew. Chem. 120 (2008) 9857–9862.
[18] L. Xiong, Y. Xu, T. Tao, J.B. Goodenough, J. Power Sources 199 (2012) 214–219.
[19] M. Richard, J. Dahn, J. Electrochem. Soc. 146 (1999) 2068–2077.
[20] C. Menachem, D. Golodnitsky, E. Peled, J. Solid State Electrochem. 5 (2001) 81–87.
[21] A. Du Pasquier, F. Disma, T. Bowmer, A. Gozdz, G. Amatucci, J.M. Tarascon, J. Electrochem. Soc. 145 (1998) 472–477.
[22] A.M. Andersson, M. Herstedt, A.G. Bishop, K. Edström, Electrochim. Acta 47 (2002) 1885–1898.
[23] K. Edström, A. Andersson, A. Bishop, L. Fransson, J. Lindgren, A. Hussenius, J. Power Sources 97 (2001) 87–91.
[24] G. Zhuang, Y. Chen, P.N. Ross, Langmuir 15 (1999) 1470–1479.
[25] T. Yoon, S. Park, J. Mun, J.H. Ryu, W. Choi, Y.-S. Kang, J.-H. Park, S.M. Oh, J. Power Sources 215 (2012) 312–316.
[26] J.-i. Yamaki, Y. Baba, N. Katayama, H. Takatsuji, M. Egashira, S. Okada, J. Power Sources 119 (2003) 789–793.
[27] J. Song, M.-H. Ryou, B. Son, J.-N. Lee, D.J. Lee, Y.M. Lee, J.W. Choi, J.-K. Park, Electrochim. Acta 85 (2012) 524–530.
[28] M.-H. Ryou, G.-B. Han, Y.M. Lee, J.-N. Lee, D.J. Lee, Y.O. Yoon, J.-K. Park, Electrochim. Acta 55 (2010) 2073–2077.
[29] M.-H. Ryou, J.-N. Lee, D.J. Lee, W.-K. Kim, J.W. Choi, J.-K. Park, Y.M. Lee, Electrochim. Acta 102 (2013) 97–103.
[30] T. Osaka, T. Momma, D. Mukoyama, H. Nara, J. Power Sources 205 (2012) 483–486.
[31] K. Wu, J. Yang, X.–Y. Qiu, J.–M. Xu, Q.–Q. Zhang, J. Jin, Q.–C. Zhuang, Electrochim. Acta 108 (2013) 841–851.
[32] H. Sasase, T. Aoki, H. Katono, K. Sanui, N. Ogata, R. Ohta, T. Kondo, T. Okano, Y. Sakurai, Makromol. Chem. Rapid Commun. 13 (1992) 577–581.
[33] Evonik Insustries Online Catalog, 2013.
[34] O. Mahendran, S. Rajendran, Ionics 9 (2003) 282–288.
[35] Y. Xu, G. Yin, Y. Ma, P. Zuo, X. Cheng, J. Power Sources 195 (2010) 2069–2073.
[36] M.-H. Ryou, J. Kim, I. Lee, S. Kim, Y.K. Jeong, S. Hong, J.H. Ryu, T.S. Kim, J.K. Park, H. Lee, Adv. Mater. 25 (2012) 1571–1576.
[37] W.-R. Liu, M.-H. Yang, H.-C. Wu, S. Chiao, N.-L. Wu, Electrochem. Solid State Lett. 8 (2005) A100–A103.
[38] S. Iwamori, N. Hasegawa, A. Uemura, T. Tanabe, I. Nishiyama, Vacuum 84 (2010) 592–596.
[39] A. Oyane, Y. Yokoyama, M. Kasahara, N. Ichinose, M. Saito, A. Ito, Mater. Sci. Eng. C 29 (2009) 1681–1686.
[40] M.M. Ramos, A.M. Stoneham, A. Sutton, Acta Metall. Mater. 41 (1993) 2105–2111.
[41] S. Zhang, Z. Xianting, W. Yongsheng, C. Kui, W. Wenjian, Surf. Coat. Tech. 200 (2006) 6350–6354.